photonics

Article

Watt-Level Diode-End-Pumped Self-Mode-Locked Tm,Ho:LLF Laser

Su Zhang *, Liheng Ma, Wen Liu, Chunsheng Sun, Hongwei Han, Qingping Hu, Shuang Zhang and Li Kai

College of Weapons Engineering, Naval University of Engineering, Wuhan 430033, China; jeremiahmax@163.com (L.M.); liusenanbei@163.com (W.L.); scs96581@163.com (C.S.); powerfire@aliyun.com (H.H.); huqingping1981@163.com (Q.H.); zhangshuangyue@sina.com (S.Z.); kaili@hust.edu.cn (L.K.)

* Correspondence: suzhang@hrbeu.edu.cn

Abstract: A diode-end-pumped self-mode-locked Tm,Ho:$LuLiF_4$ (LLF) laser is demonstrated for the first time, to the best of our knowledge. At the incident pump power of 3.4 W, the stable self-mode-locked operation of the Tm,Ho:LLF laser was realized without any additional devices in the resonator. Further increasing the incident pump power to 6.8 W, the maximum average output power of 1.07 W was achieved at 2068 nm with a pulse width of 746 ps and a repetition frequency of 468 MHz. The experimental results indicate that the Tm,Ho:LLF crystal is promising to generate the high-power self-mode-locked solid-state laser at 2 μm waveband. The self-mode-locked Tm,Ho:LLF laser has potential applications in optical communication, remote sensing, material process, and nonlinear frequency conversion.

Keywords: self-mode-locked; Tm,Ho:LLF; diode-end-pumped; watt level

Citation: Zhang, S.; Ma, L.; Liu, W.; Sun, C.; Han, H.; Hu, Q.; Zhang, S.; Kai, L. Watt-Level Diode-End-Pumped Self-Mode-Locked Tm,Ho:LLF Laser. *Photonics* **2023**, *10*, 1133. https://doi.org/10.3390/photonics10101133

Received: 7 September 2023
Revised: 29 September 2023
Accepted: 7 October 2023
Published: 10 October 2023

1. Introduction

Ultrafast laser sources emitting around 2 μm spectral region attract intense attention due to their promising applications in various fields, such as optical communication, remote sensing, laser surgery, material process, and nonlinear frequency conversion [1–10]. Moreover, such laser sources with high power and picosecond pulses can be used for improving the resolution in the laser range and reducing the damage densities in pumping optical parametric oscillators for the generation of frequency combs in the mid-IR spectral region. Especially, ultrafast 2 μm laser sources extend existing ultrafast laser material processing technology into the mid-IR region. The ultrafast 2 μm laser sources make the possibility of expanding high-precision material processing techniques to materials that are opaque in the visible and near-infrared spectral ranges but optically transparent in the 2 μm region. In the medical field, the picosecond-level pulse duration is short enough to drive tissue ablation faster than the thermal and acoustic energy transfer processes that cause damage to the surrounding tissue, but long enough to avoid tissue ionization and the risks of creating toxic free radicals and fragmenting constituent proteins. Therefore, high-power picosecond 2 μm pulse lasers are of interest for minimally invasive surgery and better than conventional medical lasers with a pulse duration longer than nanoseconds. Typically, a solid-state laser around 2 μm is achieved using singly thulium (Tm^{3+})- or holmium (Ho^{3+})-doped and Tm^{3+}, Ho^{3+} co-doped bulk materials [11–13]. Compared with the Tm^{3+}-doped laser, the Ho^{3+}-doped laser features the merits of natural emission slightly above 2 μm based on the electronic transition $_5I^7 \rightarrow {}_5I^8$ independent of the host material, which can not only avoid detrimental water vapor absorption/dispersion in the atmosphere but also realize nonlinear frequency conversion of the nonlinear crystals such as $ZnGeP_2$ [14] and orientation-patterned GaAs [15], which have high absorption losses at wavelengths shorter than 2 μm. However, the narrow-structured gain profiles of Ho^{3+}-doped laser gain materials limit the generation of ultrafast lasers in singly Ho^{3+}-doped mode-locked lasers. In addition, in terms of pump sources, Ho^{3+}-doped lasers commonly require the use of Tm^{3+}-doped solid-state or fiber lasers as the pump sources, making the overall structure more complex. Meanwhile, another approach adopting InP-based laser diodes with emissions around 1.9 μm for Ho^{3+} pumping has not yet reached the level of technological maturity. The problems of singly Tm^{3+}- or Ho^{3+}-doped lasers can be resolved by co-doping with Tm^{3+} and Ho^{3+} ions. Tm^{3+}, Ho^{3+} co-doped materials can not only combine their stimulated emissions and support ultrabroad spectra in the mode-locked regime [9,16] but also make it possible to use the widely commercial AlGaAs-based laser diodes emitting near 0.8 μm as the pump sources. Consequently, the 2 μm ultrafast pulse lasers based on Tm^{3+}, Ho^{3+} co-doped laser crystals have been widely investigated in the past few years.

To date, 2 μm ultrafast pulse lasers based on Tm^{3+}, Ho^{3+} co-doped materials have been realized by using actively and passively mode-locked methods [17–27]. In comparison with the actively mode-locked method, the passively mode-locked method of solid-state lasers possesses the advantages of compactness, low cost, reliability, and simplicity in operation. As a result, a considerable number of Tm^{3+}, Ho^{3+} co-doped passively mode-locked lasers have been demonstrated using quantum wells [18], single-walled carbon nanotubes (SWCNT) [19–21], Cr:ZnS [22], graphene [23], and semiconductor saturable absorption mirror (SESAM) [9,10,24–27] as the saturable absorbers (SAs). Nevertheless, the low damage threshold (quantum wells, SWCNT, graphene) and difficulty in manufacturing processes (SESAM) limit the application prospects of Tm^{3+}, Ho^{3+} co-doped passively mode-locked lasers. The technique of self-mode-locking (SML), which is based on the Kerr-lens effect in the gain medium and no additional modulation elements in the resonator, provides another approach to achieve ultrafast pulse lasers. Since the first SML laser was realized [28], SML has become a common ultrafast pulse generation technique in the near-infrared (IR) spectra region owing to the merits of low losses and high efficiency. As a consequence, the early research on SML mainly focused on Yb^{3+}- and Nd^{3+}-doped solid-state lasers at 1 μm waveband [29–36]. However, the realization of SML operation in mid-IR solid-state lasers is more challenging because the Kerr-lens effect is weaker in the mid-IR wavelength range than in the near-IR wavelength range [7], resulting in no reports on mid-IR SML until the first Kerr-lens SML Tm^{3+}:Sc_2O_3 laser at 2.1 μm was demonstrated in 2017 [37]. Therefore, up to now, only a few works have been reported on SML solid-state lasers at 2 μm waveband. In 2017, Tokurakawa et al. reported on the first Kerr-lens SML Tm^{3+}:Sc_2O_3 laser at 2.1 μm by exploiting a standard *Z*-shaped cavity and an Er:Yb fiber master oscillator power amplifier at 1611 nm as an in-band pump source. The maximum average output power was 1 W with a pulse repetition frequency of 95 MHz [37]. In 2019, by adopting a Tm^{3+}-doped fiber laser, an SML Ho:YAG laser at 2128.36 nm was achieved. The maximum average output power was 4.27 W with a pulse repetition frequency of 656.6 MHz and a pulse width of 471.6 ps [38]. Subsequently, several SML lasers were successfully realized using other Tm^{3+}-doped and Ho^{3+}-doped laser crystals [39–41]. According to the advantages of Tm^{3+}, Ho^{3+} co-doped in mode-locked lasers mentioned above, Tm^{3+}, Ho^{3+} co-doped laser gain media have been investigated in realizing SML lasers. For example, the SML Tm^{3+}, Ho^{3+} co-doped laser composed of a Tm,Ho:CALGO crystal pumped by a Ti:sapphire laser [42], which delivered mode-locked pulses at 2038 nm with a maximum average output power of 423 mW. It is worth noting that the above research about Tm^{3+}, Ho^{3+} co-doped SML solid-state lasers near 2 μm mainly focuses on Tm^{3+}, Ho^{3+} co-doped oxide materials. However, there is no report on 2 μm SML solid-state lasers based on Tm^{3+}, Ho^{3+} co-doped fluoride materials so far.

Among the Tm^{3+}, Ho^{3+} co-doped materials, Tm,Ho:$LuLiF_4$ (LLF) is a kind of excellent laser crystal for generating 2 μm lasers, benefited by high birefringence, a long upper state lifetime, a large emission cross-section, and favorable thermo-optical and thermos-mechanical properties [43]. Its thermal conductivity (*a*-axis), linear expansion coefficient (*a*-axis), and thermal coefficient of refractive index dn/dT (π-polarization) are 5 $Wm^{-1}K^{-1}$, 13.6×10^{-6} K^{-1}, and -6×10^{-6} K^{-1}, respectively [44]. In the past years, the continuous wave (CW), Q-switched, and passive mode-locking of Tm,Ho:LLF lasers have been realized [22,26,45]. In 2017, Zhang et al. reported on a diode-end-pumped passively Q-switched mode-locking Tm,Ho:LLF laser using a Cr:ZnS saturable absorber. The maximum average output power was 145 mW, and the width of the mode-locked pulse was estimated to be less than 682 ps with a 250 MHz repetition frequency within a Q-switched pulse envelope of about 700 ns [22]. Significantly, the implementation of the passively mode-locked Tm,Ho:LLF laser indicates that the Tm,Ho:LLF crystal is a promising candidate for realizing mode-locked lasers in the 2 μm spectra region. Nevertheless, to the best of our knowledge, the SML Tm,Ho:LLF laser has not been reported to date.

In this paper, an SML Tm,Ho:LLF laser at 2068 nm is demonstrated for the first time, to the best of our knowledge. The threshold pump power of the SML Tm,Ho:LLF laser was as low as 3.4 W, and the maximum average output power of 1.07 W was achieved at the incident pump power of 7.8 W. The pulse repetition frequency and pulse width were 468 MHz and 746 ps, respectively.

2. Experimental Setup

A schematic diagram of the diode-end-pumped SML Tm,Ho:LLF laser is shown in Figure 1. A Tm,Ho:LLF crystal cut along the *a*-axis with the dimensions of 4 mm × 4 mm × 2.5 mm and the dopant concentrations of 5 at.% Tm^{3+} and 0.5 at.% Ho^{3+} was used as the laser gain medium. Both end surfaces of the crystal were coated with antireflection at 792 nm and 2 μm. The laser crystal was wrapped with indium foil and tightly mounted into a brass sink heat, which was maintained at the cooling temperature of 10 °C with a thermoelectric cooler. The pump source was a fiber-coupled laser diode (LD) with a central wavelength of 792 nm and a maximum output power of 50 W. The diameter and numerical aperture of the fiber core were 400 μm and 0.22, respectively. The pump beam was focused into the Tm,Ho:LLF laser crystal with a 1:1 coupling optics system yielding a pump spot radius of 200 μm in the laser gain medium. A simple plane-concave cavity configuration consisting of the input plat mirror M1 and output coupler M2 was utilized for achieving the SML Tm,Ho:LLF laser in the experiment, and the optical length of the cavity was approximately 320 mm. The incident facet of the input plat mirror M1 was coated with antireflection at 792 nm, and the other facet was coated with high transmittance at 792 nm and high reflection around 2 μm. A plane concave mirror M2 with a 300 mm curvature radius was chosen as the output coupler with 94% reflection around 2 μm.

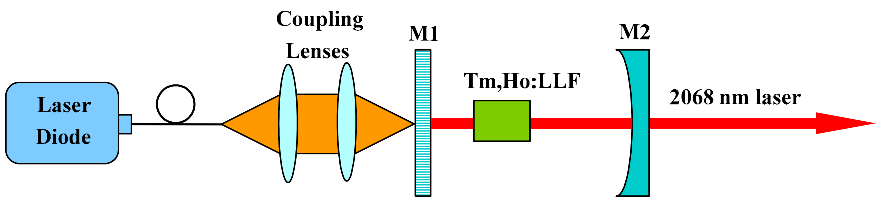

Figure 1. Experimental setup of the SML Tm,Ho:LLF laser.

In the experiment, a power meter (Molectron PM10) was used to measure the average output power of the Tm,Ho:LLF laser. The optical spectrum of the output laser was analyzed with a spectrum analyzer (Bristol Instruments 721A). The temporal characteristics of the SML laser were detected with a high-speed InGaAs photodetector (Electro-Optics Technology, ET-5000) with a bandwidth of 12.5 GHz, and the output signals were recorded with a digital oscilloscope (Keysight Technologies MSOS804A) with an electrical bandwidth of 8 GHz and a sampling rate of 20 GSa/s. The output signals of the photodetector were also analyzed with a ratio frequency spectrum analyzer (Rohde & Schwarz, FSEK30) with a bandwidth of 40 GHz. For evaluating the beam quality of the output laser, a beam analyzer (Electrophysics, Micron Viewer 7920A) was applied to record the transverse output beam profile of the SML Tm,Ho:LLF laser.

3. Results and Discussion

Initially, the maximum CW operating performance of the Tm,Ho:LLF laser was investigated. The CW output power with respect to the pump power is shown in Figure 2.

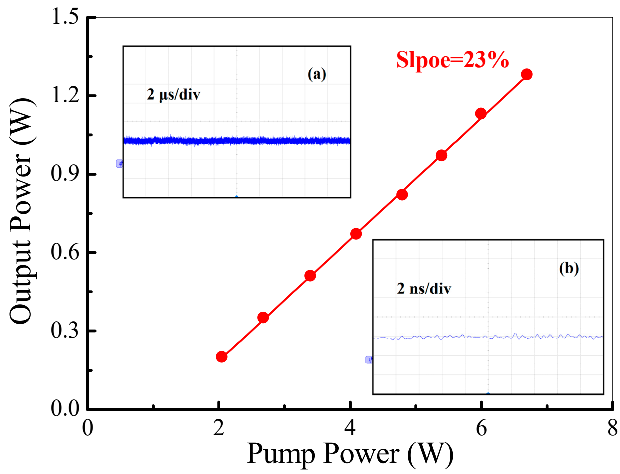

Figure 2. Output power as a function of incident pump power for the CW Tm,Ho:LLF laser. Insets: the oscilloscope traces of the CW Tm,Ho:LLF laser with two different time spans of (**a**) 20 μs and (**b**) 20 ns.

When the incident pump power was lower than 2 W, the laser resonator was in an unstable state and the laser did not oscillate. Increasing the pump power to 2 W, the laser cavity turned to be stable, resulting from the effect of the thermal lens; meanwhile, the output power jumped from 0 to 0.2 mW. By gradually increasing the pump power, the output power increased linearly with the pump power. In addition, the laser always operated in the CW state in the process of changing incident pump power. The real-time temporal behaviors of the output laser for various pump powers displayed no self-pulsing or mode-locked pulsing phenomenon, as illustrated in the insets of Figure 2, which verified the CW operation of the Tm,Ho:LLF laser. The output power reached a maximum of 1.28 W at the incident pump power of 6.8 W, corresponding to a slope efficiency of 23%.

On the basis of the maximum CW operation of the Tm,Ho:LLF laser, by slightly tilting the output coupler M2, finely adjusting the pump spot position in the Tm,Ho:LLF crystal, and carefully regulating the distance between the input mirror M1 and the Tm,Ho:LLF crystal, the SML operation of the Tm,Ho:LLF laser was successfully realized. Figure 3a indicates the average output power of the SML Tm,Ho:LLF laser as a function of the incident pump power. It can be found that the average output power linearly increased with the incident pump power. In the process of increasing pump power from 2 W to 2.68 W, the Tm,Ho:LLF laser operated in the CW state. Further increasing pump power, the Tm,Ho:LLF laser went into the unstable SML regime, and the SML pulses were extremely unstable with weak peak-to-peak stability. Moreover, it should be mentioned that the Tm,Ho:LLF laser directly switched from the CW mode to the SML state, and the self-pulsing phenomenon that appeared in the SML Tm:YAG laser was not observed [39]. The Tm,Ho:LLF laser operates slightly above 2 μm avoiding the water vapor absorption, which might result in the absence of self-pulsing for the Tm,Ho:LLF laser in the process of switching operation states. With the incident pump power scaling up to 3.4 W, the stable SML operation of the Tm,Ho:LLF laser was realized. Compared with the SML Tm:YAG laser, the threshold pump power of the SML Tm,Ho:LLF laser was much lower because there was no need to suppress the self-pulsing. The maximum average output power was found to be 1.07 W at the incident pump power of 6.8 W, and the corresponding slope efficiency was 19.6%. In the passively mode-locked Tm,Ho:LLF laser based on the SESAM, the maximum average output power and slope efficiency were 234 mW and 12.5%, respectively [26]. In contrast, the SML Tm,Ho:LLF laser had a higher efficiency because there are no additional mode-locking devices in the resonator, so the cavity losses were significantly decreased.

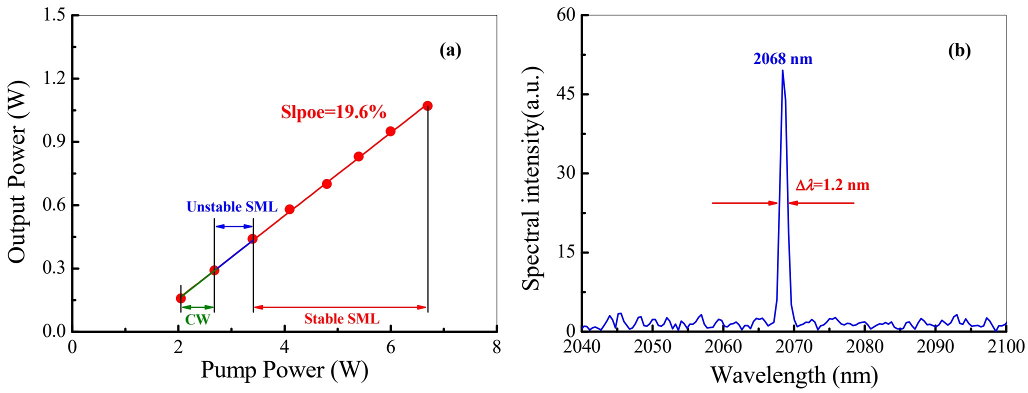

Figure 3. (**a**) Average output power as a function of incident pump power for the SML Tm,Ho:LLF laser. (**b**) Output spectrum for the SML Tm,Ho:LLF laser.

Figure 3b describes the optical spectrum of the SML Tm,Ho:LLF laser with respect to the incident pump power of 6.8 W. It can be seen from Figure 3b that the central wavelength of the SLM Tm,Ho:LLF laser was 2068 nm with a spectral bandwidth of 1.2 nm. A Glan prism was used to measure the polarization of the SML Tm,Ho:LLF laser. It was found that the output laser was π-polarized along the *c*-axis of the laser crystal.

The real-time temporal behavior of the SML Tm,Ho:LLF laser recorded at the incident pump power of 6.8 W for two different time spans of 20 µs and 20 ns is shown in Figure 4, which manifested the stability of the SML Tm,Ho:LLF laser. From Figure 4b, it can be observed that the time interval of two neighboring pulses is 2.1 ns, which means the pulse repetition rate of the SML Tm,Ho:LLF laser is approximately 468 MHz, corresponding to the fundamental repetition rate of the 320 mm optical cavity length. The pulse width at the maximum output power of 1.07 W was measured to be 746 ps, which is close to the real value because the MSOS804A digital oscilloscope (with an electrical bandwidth of 8 GHz) and the ET-5000 high-speed InGaAs PIN photodetector (with a bandwidth of 12.5 GHz) are able to measure such a pulse with over 125 ps.

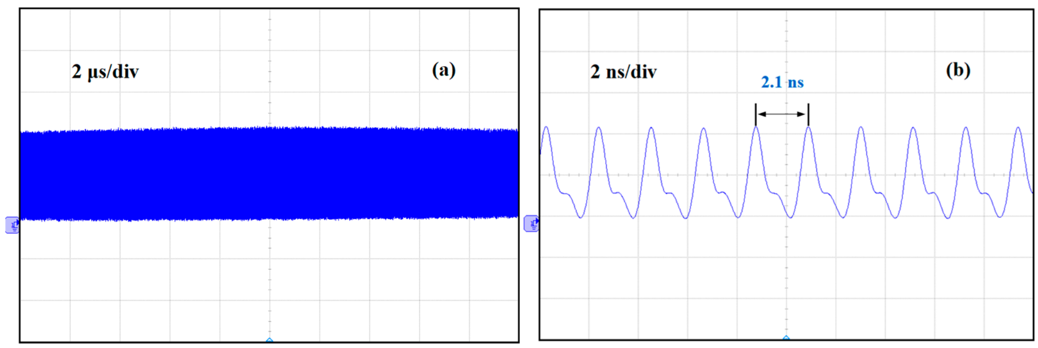

Figure 4. The temporal pulse trains of the SML Tm,Ho:LLF laser with two different time spans of (**a**) 20 µs and (**b**) 20 ns, respectively.

It should be noted that in the previous research on the 2 µm Tm^{3+}, Ho^{3+} co-doped mode-locked laser, a Ti:sapphire laser was commonly used as the pump source due to its good beam quality and high brightness. Compared with the Ti:sapphire laser, the LD pump source has the advantages of low cost and compactness. However, the intrinsic weak brightness of LD makes it difficult for the pump mode to match the tightly focused laser mode, resulting in the challenges of suppressing the Q-switched mode-locking and obtaining a strong enough Kerr-lens effect for generating ultrafast pulses. As a result, the laser pulse duration of an LD-pumped Tm^{3+}, Ho^{3+} co-doped mode-locked laser is mainly in the range of picosecond [10], corresponding to a narrow mode-locking spectrum. Consequently, the pulse duration of the LD-pumped SML Tm,Ho:LLF laser achieved in this research is much longer than other mode-locked Tm^{3+}, Ho^{3+} co-doped lasers pumped by a Ti:sapphire laser pump source [9,27,42].

To further evaluate the stability of the SML Tm,Ho:LLF laser, the radio-frequency (RF) spectrum was also measured at the incident pump power of 6.8 W, as shown in Figure 5a. It can be seen from Figure 5a that the RF spectrum has a signal–noise ratio of ~41 dB, revealing the relatively high stability of the SML Tm,Ho:LLF laser. Furthermore, there are not any side peaks near the center peak of 468 MHz, as illustrated in Figure 5a, which further proves that the Tm,Ho:LLF laser operated in the mode-locking mode instead of the Q-switched mode-locking state or relaxation oscillation. In addition, the pulse repletion rate of ~468 MHz is in agreement with the laser cavity length of 320 mm.

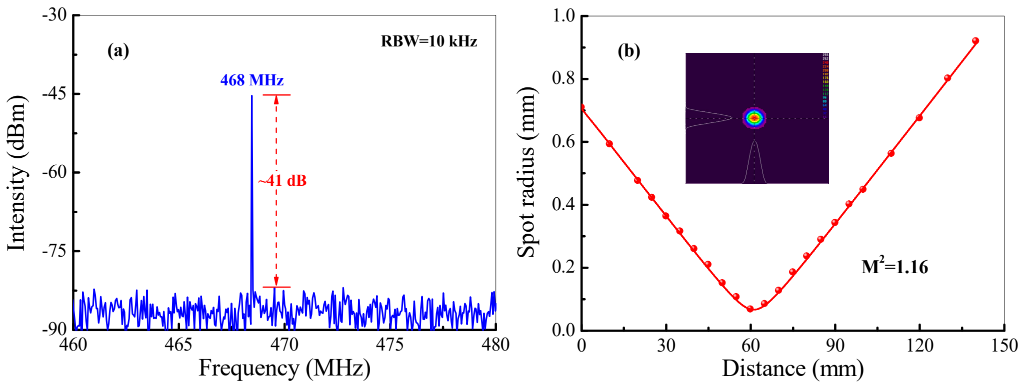

Figure 5. (**a**) Fundamental ratio frequency spectrum of the SML Tm,Ho:LLF laser with the resolution bandwidth of 10 kHz. (**b**) Beam radius of the SML Tm,Ho:LLF laser as a function of distance, and the inset shows the transverse beam profile.

The transverse output beam profile of the SML Tm,Ho:LLF laser at the incident pump power of 6.8 W was measured, as shown in the inset in Figure 5b. The output beam was close to the fundamental transverse electromagnetic mode (TEM_{00}). The beam radii at different positions along the beam propagation direction were measured using the method of traveling knife-edge, as shown in Figure 5b, and the fitted beam quality factor for the SML Tm,Ho:LLF laser was 1.16.

4. Conclusions

We demonstrated a diode-end-pumped SML Tm,Ho:LLF laser at 2068 nm with a simple two-mirror cavity for the first time, to the best of our knowledge. The threshold pump power of the stable SML Tm,Ho:LLF laser was as low as 3.4 W, and the maximum average output power was 1.07 W at the incident pump power of 6.8 W, corresponding to a slope efficiency of 19.6%. The pulse width and repetition frequency were 746 ps and 468 MHz, respectively. The output laser had a good beam quality with an M^2 factor of 1.16. The experimental results indicate that the Tm,Ho:LLF crystal is a promising gain medium for realizing the SML solid-state laser in the 2 µm wavelength range. The SML Tm,Ho:LLF laser has potential applications in optical communication, remote sensing, material processing, and nonlinear frequency conversion.

Author Contributions: Conceptualization, S.Z. (Su Zhang); data curation, S.Z. (Su Zhang), L.M., W.L. and C.S.; investigation, S.Z. (Su Zhang), L.M., H.H., Q.H. and S.Z. (Shuang Zhang); writing—review and editing, S.Z. (Su Zhang), L.M., W.L. and L.K.; formal analysis, S.Z. (Su Zhang); writing—original draft preparation, S.Z. (Su Zhang); project administration, S.Z. (Su Zhang) and L.M.; supervision, S.Z. (Su Zhang). All authors have read and agreed to the published version of the manuscript.

Funding: This work was supported by the Independent Scientific Research Project of the Naval University of Engineering (2022507010).

Institutional Review Board Statement: Not applicable.

Informed Consent Statement: Not applicable.

Data Availability Statement: Data underlying the results presented in this paper are not publicly available at this time but may be obtained from the authors upon request.

Conflicts of Interest: The authors declare no conflict of interest.

References

1. Schliesser, A.; Picqué, N.; Hänsch, N.T. Mid-infrared frequency combs. *Nat. Photonics* **2012**, *6*, 440–449.
2. Singh, U.N.; Walsh, B.M.; Yu, J.; Petros, M.; Kavaya, M.J.; Refaat, T.F.; Barnes, N.P. Twenty years of Tm:Ho:YLF and LuLiF laser development for global wind and carbon dioxide active remote sensing. *Opt. Mater. Express* **2015**, *5*, 827–837. [CrossRef]
3. Rieker, G.B.; Giorgetta, F.R.; Swann, W.C.; Kofler, J.; Zolot, A.M.; Sinclair, L.C.; Baumann, E.; Cromer, C.; Petron, G.; Sweeney, C.; et al. Frequency-comb-based remote sensing of greenhouse gases over kilometer air paths. *Optica* **2014**, *1*, 290–298. [CrossRef]
4. Amini-Nik, S.; Kraemer, D.; Cowan, M.L.; Gunaratne, K.; Nadesan, P.; Alman, B.A.; Dwayne Miller, R.J. Ultrafast Mid-IR Laser Scalpel: Protein Signals of the Fundamental Limits to Minimally Invasive Surgery. *PLoS ONE* **2010**, *5*, e13053. [CrossRef]
5. Haq, B.S.; Khan, H.U.; Alam, K.T.; Mateenullah, M.; Attaullah, S.; Zari, I. Femtosecond pulsed laser ablation of polyimide at oblique angles for medical applications. *Appl. Opt.* **2015**, *54*, 7413–7418. [CrossRef] [PubMed]
6. Godard, A. Infrared (2–12 μm) solid-state laser sources: A review. *C. R. Phys.* **2007**, *8*, 1100–1128.
7. Ma, J.; Qin, Z.P.; Xie, G.Q.; Qian, L.J.; Tang, D. Review of mid-infrared mode-locked laser sources in the 2.0 μm–3.5 μm spectral region. *Appl. Phys. Rev.* **2019**, *6*, 021317.
8. Parsa, S.; Kumar, S.C.; Nandy, B.; Ebrahim-Zadeh, M. Yb-fiber-pumped, high-beam-quality, idler-resonant mid-infrared picosecond optical parametric oscillator. *Opt. Express* **2019**, *27*, 25436–25444. [CrossRef]
9. Wang, L.; Chen, W.D.; Zhao, Y.G.; Loiko, P.; Mateos, X.; Guina, M.; Pan, Z.B.; Mero, M.; Griebner, U.; Petrov, V. Sub-50 fs pulse generation from a SESAM mode-locked Tm, Ho-codoped calcium aluminate laser. *Opt. Lett.* **2021**, *46*, 2642–2645. [CrossRef]
10. Zhao, Y.T.; Li, Y.; Zhao, S.Z.; Liu, Y.Z.; Li, T.; Hu, P.; Mao, J.J.; Yang, K.J.; Wang, C.; Feng, T.L. Diode-pumed Tm^{3+}, Ho^{3+} co-doped GAGG mode-locking laser near the 2.1 μm wavelength region. *Opt. Express* **2022**, *30*, 13890–13897. [CrossRef]
11. Antoine, B.; Oliver, J.P.C.; Daniel, M.; Daniel, E.M.J. Comparative study of high power Tm:YLF and Tm:LLF slab lasers in continuous wave regime. *Opt. Express* **2018**, *26*, 10559–10572.
12. Dai, T.; Wang, Y.P.; Wu, X.S.; Wu, J.; Yao, B.Q.; Ju, Y.L.; Shen, Y.J. An injection-seeded Q-switched Ho:YLF laser by a tunable single-longitudinal-mode Tm, Ho:YLF laser at 2050.96 nm. *Opt. Laser Technol.* **2018**, *106*, 7–11. [CrossRef]
13. Zhang, X.L.; Zhang, S.; Huang, J.J.; Ni, K.B. Theoretical end experimental investigation of polarization coexistence and switching in an optical bistability Tm, Ho:LLF laser. *Opt. Express* **2018**, *26*, 18783–18789. [CrossRef] [PubMed]
14. Wang, L.; Xing, T.L.; Hu, S.W.; Wu, X.Y.; Wu, H.X.; Wang, J.Y.; Jiang, H.H. Mid-infrared ZGP-OPO with a high optical-to-optical conversion efficiency of 75.7%. *Opt. Express* **2017**, *25*, 3373–3380. [CrossRef] [PubMed]
15. Smolski, V.O.; Vasilyev, S.; Schunemann, P.G.; Mirov, S.B.; Vodopyanov, K.L. Cr:ZnS laser-pumped subharmonic GaAs optical parametric oscillator with the spectrum spanning 3.6–5.6 μm. *Opt. Lett.* **2015**, *40*, 2906–2908. [CrossRef]
16. Pan, Z.B.; Loiko, P.; Wang, Y.C.; Zhao, Y.G.; Yuan, H.L.; Tang, K.Y.; Dai, X.J.; Cai, H.Q.; Serres, J.M.; Slimi, S.; et al. Disordered Tm^{3+}, Ho^{3+}-codoped CNGG garnet crystal: Towards efficient laser materials for ultrashort pulse generation at ~2 μm. *J. Alloys Compd.* **2021**, *853*, 157100. [CrossRef]
17. Gatti, D.; Galzerano, G.; Toncelli, A.; Tonelli, M.; Laporta, P. Actively mode-locked Tm-Ho:$LiYF_4$ and Tm-Ho:BaY_2F_8 lasers. *Appl. Phys. B* **2007**, *86*, 269–273. [CrossRef]
18. Yang, K.; Bromberger, H.; Ruf, H.; Schäfer, H.; Neuhaus, J.; Dekorsy, T.; Grimm, C.V.; Helm, M.; Briermann, K.; Künzel, H. Passively mode-locked Tm,Ho:YAG laser at 2 μm based on saturable absorption of intersubband transitions in quantum wells. *Opt. Express* **2010**, *18*, 6537–6544. [CrossRef]
19. Aleksandrov, V.; Gluth, A.; Petrov, V.; Buchvarov, I.; Choi, S.Y.; Kim, M.H.; Rotermund, F.; Mateos, X.; Díaz, F.; Griebner, U. Tm,Ho:$KLu(WO_4)_2$ laser mode-locked near 2 μm by single-walled carbon nanotubes. *Opt. Express* **2014**, *22*, 26872–26877. [CrossRef]
20. Pan, Z.; Wang, Y.; Zhao, Y.; Kowalczyk, M.; Sotor, J.; Yuan, H.; Zhang, Y.; Dai, X.; Cai, H.; Bae, J.E.; et al. Sub-80 fs mode-locked Tm,Ho-codoped disordered garnet crystal oscillator operating at 2081 nm. *Opt. Lett.* **2018**, *43*, 5154–5157. [CrossRef]
21. Pan, Z.; Wang, L.; Bae, J.E.; Rotermund, F.; Wang, Y.; Zhao, Y.; Loiko, P.; Mateos, X.; Griebner, U.; Petrov, V.; et al. SWCNT-SA mode-locked Tm,Ho:LCLNGG laser. *Opt. Express* **2021**, *29*, 40323–40332. [CrossRef]
22. Zhang, X.L.; Luo, Y.; Wang, T.H.; Dai, J.F.; Zhang, J.X.; Li, J.; Cui, J.H.; Huang, J.J. Cr:ZnS saturable absorber passively Q-switched mode-locking Tm,Ho:LLF laser. *Appl. Opt.* **2017**, *56*, 2973–2977. [CrossRef] [PubMed]
23. Paris, M.; Tyazhev, A.; Loiko, P.; Soulard, R.; Doualan, J.; Guillemot, L.; Braud, A.; Godin, T.; Camy, P.; Hideur, A. Passively mode-locked diode-pumped Tm,Ho:$LiYF_4$ laser. *Laser Phys. Lett.* **2020**, *17*, 045801. [CrossRef]

24. Yang, K.J.; Heinecke, D.C.; Kölbl, C.; Dekorsy, T.; Zhao, S.Z.; Zheng, L.H.; Xu, J.; Zhao, G.J. Mode-locked Tm,Ho:YAP laser around 2.1 µm. *Opt. Express* **2013**, *21*, 1574–1580. [CrossRef] [PubMed]
25. Aleksandrov, V.; Gluth, A.; Petrov, V.; Buchvarov, I.; Steinmeyer, G.; Paajaste, J.; Suomalainen, S.; Härkönen, A.; Guina, M.; Mateos, X.; et al. Mode-locked Tm,Ho:KLu(WO_4)$_2$ laser at 2060 nm using InGaSb-base SESAMs. *Opt. Express* **2015**, *23*, 4614–4619. [CrossRef] [PubMed]
26. Ling, W.J.; Xia, T.; Dong, Z.; You, L.F.; Zhang, M.X.; Zuo, Y.Y.; Li, K.; Liu, Q.; Lu, F.P. Passively mode-locked Tm,Ho:LLF laser at 1895 nm. *J. Opt.* **2019**, *48*, 209–213. [CrossRef]
27. Zhao, Y.; Wang, Y.; Zhang, X.; Mateos, X.; Pan, Z.; Loiko, P.; Zhou, W.; Xu, X.; Xu, J.; Shen, D.; et al. 87 fs mode-locked Tm,Ho:$CaYAlO_4$ laser at ~2043 nm. *Opt. Lett.* **2018**, *43*, 915–918. [CrossRef]
28. Spence, D.E.; Kean, P.N.; Sibbett, W. 60-fsec pulse generation from a self-mode-locked Ti:sapphire laser. *Opt. Lett.* **1991**, *16*, 42–44. [CrossRef]
29. Xie, G.Q.; Tang, D.Y.; Zhao, L.M.; Qian, L.J.; Ueda, K. High-power self-mode-locked Yb:Y_2O_3 ceramic laser. *Opt. Lett.* **2007**, *32*, 2741–2743. [CrossRef]
30. Zhuang, W.Z.; Chang, M.T.; Liang, H.C.; Chen, Y.F. High-power high-repetition-rate subpicosecond monolithic Yb:KGW laser with self-mode locking. *Opt. Lett.* **2013**, *38*, 2596–2599. [CrossRef]
31. Zhang, J.; Han, H.; Tian, W.; Lv, L.; Wang, Q.; Wei, Z. Diode-pumped 88-fs Kerr-lens mode-locked Yb:$Y_3Ga_5O_{12}$. *Opt. Express* **2013**, *21*, 29867–29873. [CrossRef] [PubMed]
32. Tian, W.; Wang, Z.; Wei, L.; Peng, Y.; Zhang, J.; Zhu, Z.; Zhu, J.; Han, H.; Jia, Y.; Zheng, L.; et al. Diode-pumped Kerr-lens mode-locked Yb:LYSO laser with 61 fs pulse duration. *Opt. Express* **2014**, *22*, 19040–19046. [CrossRef] [PubMed]
33. Huang, Y.J.; Tzeng, Y.S.; Tang, C.Y.; Huang, Y.P.; Chen, Y.F. Tunable GHz pulse repetition rate operation in high-power TEM_{00}-mode Nd:YLF lasers at 1047 nm and 1053 nm with self mode locking. *Opt. Express* **2012**, *20*, 18230–18237. [CrossRef] [PubMed]
34. Chen, W.D.; Li, Y.Y.; Zhang, G.; Huang, Y.H.; Chen, Z.Q. Spontaneous picosecond pulse generation in a diode-pumped Nd:YAP laser. *Opt. Express* **2013**, *21*, 25091–25098. [CrossRef]
35. Tuan, P.H.; Tsai, M.C.; Chen, Y.F. Exploiting birefringent thermal lensing effect to manipulate polarization states of an Nd:YVO_4 self-mode-locked laser. *Opt. Express* **2017**, *25*, 29000–29009. [CrossRef]
36. Liang, H.C.; Wu, S.C. Diode-pumped orthogonally polarized self-mode-locked Nd:YLF lasers subject to gain competition and thermal lensing effect. *Opt. Express* **2017**, *25*, 13697–13704. [CrossRef]
37. Tokurakawa, M.; Fujita, E.; Kränkel, C. Kerr-lens mode-locked Tm^{3+}:Sc_2O_3 single-crystal laser in-band pumped by an Er:Yb fiber MOPA at 1611 nm. *Opt. Lett.* **2017**, *42*, 3185–3187. [CrossRef] [PubMed]
38. Zhang, G.J.; Zhang, H.K.; Fu, X.; Liu, Q. Compact Ho:YAG laser at 2.1 µm mode locked by re-absorption. *IEEE Photonics Technol. Lett.* **2019**, *31*, 222–225. [CrossRef]
39. Cho, C.Y.; Chen, Y.F.; Zhang, G.; Chen, W.D.; Liang, H.C. Exploring the self-mode locking of the 2 µm Tm:YAG laser suppression of the self-pulsing dynamic. *Opt. Lett.* **2017**, *42*, 5226–5229. [CrossRef]
40. Zhao, Y.; Wang, L.; Chen, W.; Loiko, P.; Wang, Y.; Pan, Z.; Yang, H.; Jing, W.; Huang, H.; Liu, J.; et al. Kerr-lens mode-locked Tm-doped sesquioxide ceramic laser. *Opt. Lett.* **2021**, *46*, 3428–3431. [PubMed]
41. Yao, W.; Wang, Y.; Ahmed, S.; Hoffmann, M.; Delden, M.V.; Musch, T.; Saraceno, C.J. Low-noise, 2-W average power, 112-fs Kerr-lens mode-locked Ho:CALGO laser at 2.1 µm. *Opt. Lett.* **2023**, *48*, 2801–2804. [CrossRef] [PubMed]
42. Wang, L.; Petrov, V.; Griebner, U.; Zhang, G.; Loiko, P.; Mateos, X.; Bae, J.E.; Rotermund, F.; Xu, X.; Major, A.; et al. Kerr-lens mode-locked Tm,Ho:CALGO laser. In Proceedings of the 2022 Conference on Lasers and Electro-Optics (CLEO), San Jose, CA, USA, 15–20 May 2022. Technical Digest Series (Optica Publishing Group, 2022), paper SF1B.2.
43. Walsh, B.M.; Barnes, N.P.; Petros, M.; Yu, J.; Singh, U.N. Spectroscopy and modeling of solid state lanthanide lasers: Application to trivalent Tm^{3+} and Ho^{3+} in $YLiF_4$ and $LuLiF_4$. *J. Appl. Phys.* **2004**, *95*, 3255–3271.
44. Aggarwal, R.L.; Ripin, D.J.; Ochoa, J.R.; Fan, T.Y. Measurement of thermos-optic properties of $Y_3Al_5O_{12}$, $Lu_3Al_5O_{12}$, $YAlO_3$, $LiYF_4$, $LiLuF_4$, BaY_2F_8, KGd(WO_4)$_2$, and KY(WO_4)$_2$ laser crystals in the 80-300 K temperature range. *J. Appl. Phys.* **2005**, *98*, 103514. [CrossRef]
45. Zhang, X.L.; Yu, L.; Zhang, S.; Li, L.; Zhao, J.Q.; Cui, J.H. Diode-pumped continuous wave and passively Q-switched Tm,Ho:LLF laser at 2 µm. *Opt. Express* **2013**, *21*, 12629–12634. [CrossRef]